Efficient High-Resolution 3-D Channel Sounding

Martin Haardt,[1] *Christopher Brunner,*[1,2] *and Josef A. Nossek*[2]

1. Siemens AG, Mobile Networks, OEN MN P 36
Hofmannstr. 51, D-81359 Munich, Germany
Phone: +49 (89) 722-29480, Fax: +49 (89) 722-44958
E-mail: Martin.Haardt@oen.siemens.de

2. Institute of Network Theory and Circuit Design
Munich University of Technology, D-80290 Munich, Germany
Phone: +49 (89) 289-28511, Fax: +49 (89) 289-28504
E-Mail: chbr@nws.e-technik.tu-muenchen.de

Abstract – **The detailed knowledge of the directional characteristics of the mobile radio channel is required to develop directional channel models and to design efficient smart antenna concepts for future mobile radio systems. In this paper, we present an efficient high-resolution scheme to estimate the dominant wavefronts in terms of their two-dimensional arrival angles (azimuth and elevation) and their corresponding propagation delays. Here, the chip waveform of the sounding sequence and the correlation matrix of the (colored) additive noise are taken into account. To achieve these goals, 3-D Unitary ESPRIT is modified to cope with colored noise and is applied to the measurements of a uniform rectangular array in the space-frequency domain. Automatic pairing of the 3-D estimates is obtained by computing the simultaneous Schur decomposition of three real-valued, non-symmetric matrices. This closed-form procedure neither requires any search nor any other heuristic pairing strategy. Due to the joint estimation of these 3-D parameters, the presented 3-D channel sounder outperforms previously proposed methods. Applications of this algorithm in direct sequence CDMA systems are also discussed briefly.**

1. Introduction

Spatio-temporal radio channel measurements that include the dominant directions of arrival (DOAs) and the corresponding propagation delays are desired in a variety of applications like sonar, radar, and cellular communications. They are required to design efficient smart antenna concepts which exploit the inherent spatial diversity of the radio channel to achieve a significant increase of the spectral efficiency. Two-dimensional (2-D) antenna array geometries at the base station of a cellular communication system allow the estimation of azimuth as well as elevation angles of the dominant wavefronts that impinge on the array. Taking the elevation into account facilitates the reduction of the near-far problem in cellular radio systems. This is particularly important for direct sequence CDMA systems.

To circumvent the development and implementation of new hardware for vector channel sounding, measurement concepts based on conventional single channel measurement techniques have been developed. One method relies on angular scanning of the directional electromagnetic wave field by means of a slowly rotating narrow beam receiver antenna. At Siemens, a rotating antenna sounding campaign was carried out in urban, suburban, and rural macro-cellular environments in the Munich area at 1840 MHz [6]. To overcome the angular resolution limit inherent in rotating antenna experiments due to the physical antenna aperture size, a synthetic aperture or virtual array sounding may be used. Measurement concepts using 2-D array sounding algorithms were proposed in [1, 2, 10]. They are based on virtual arrays to increase the antenna aperture and estimate the azimuth angles along with the corresponding propagation delays of the dominant wavefronts. Reference [1] describes a computationally rather demanding maximum likelihood approach, whereas efficient subspace approaches based on 2-D Unitary ESPRIT are presented in [2, 10]. The 2-D channel sounder described in [10] provides automatically paired azimuth and propagation delay estimates of the dominant multipath components. It has already been employed successfully in several field experiments conducted by Deutsche Telekom. In [2], the authors describe wideband direction-selective downlink sounding results achieved by adopting a 2-D virtual array concept for mobile reception at different mobile positions. In several field experiments conducted by France Telecom in Paris, France, this algorithm has been employed successfully. Here, high-resolution estimates of the 2-D directions of arrival (azimuth and elevation) of the dominant propagation paths were determined by solving the two-dimensional harmonic retrieval problem for each estimated impulse response tap delay separately.

The wideband high-resolution 3-D channel sounding algorithm proposed in this paper may also be used for such virtual array sounding applications. Alternatively, it can be applied to the noise-corrupted measurements of a physical 2-D antenna array. This new joint 3-D channel sounding scheme outperforms the algorithms of [1, 2, 10] in several areas. In [2], the channel impulse response is estimated for each sensor separately. Then the two-dimensional DOAs are estimated for each delay tap independently. This causes a degradation of the temporal resolution due to the rather coarse spacing of the taps. Therefore, we apply 3-D Unitary ESPRIT to the measurements of a uniform rectangular array in the frequency domain and jointly estimate the 2-D arrival angles along with the corresponding propagation delays of the dominant multipath components. As in the 1-D case [4], the algorithm is formulated in terms of real-valued computations throughout. Automatic pairing of the 3-D estimates is achieved by computing the simultaneous Schur decomposition of three real-valued, non-symmetric matrices. This closed-form procedure neither requires any search nor any other heuristic pairing strategy [3, 5]. By jointly estimating the two-dimensional arrival angles and the corresponding propagation delays, the proposed 3-D channel sounder is able to resolve more dominant wavefronts than there are antenna elements. Moreover, it avoids difficulties in cases where two or more wavefronts have equal arrival angles or delays. In [5], it has been shown that the performance of 3-D Unitary ESPRIT is very close to the Cramér-Rao lower bound. Finally, the (complex) amplitudes of the dominant multipath components are estimated in the space-time domain by taking the estimated 2-D arrival angles and the estimated delays into account. This improves the estimation accuracy of the amplitudes as well.

2. 3-D Channel Sounding

2.1. 3-D Data Model

To measure the propagation characteristics of the radio channel, assume that the transmitter emits a sounding signal $s(t)$ consisting of a repeatedly transmitted (spreading) sequence $w(t)$, where

$$s(t) = \sum_{n=-\infty}^{\infty} w(t - nT) \text{ and } w(t) = \sum_{m=1}^{N_c} d_m p(t - mT_c). \quad (1)$$

The spreading sequence $w(t)$ is composed of N_c (complex) chips d_m, $1 \leq m \leq N_c$, weighted by the chip waveform $p(t) \in \mathbb{R}$. If the chips are of duration T_c, the spreading sequence $w(t)$ is of length $T = N_c T_c$. Moreover, we define another sequence b_m of length N_c such

0-7803-4320-4/98/$5.00 © 1998 IEEE

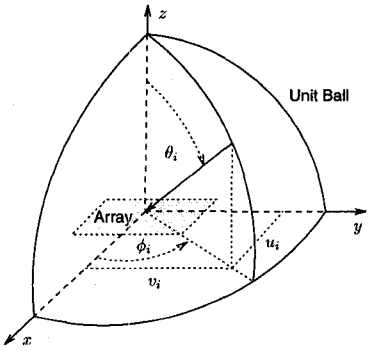

Figure 1: Definitions of azimuth ($-180° < \phi_i \leq 180°$) and elevation ($0° \leq \theta_i \leq 90°$).

that the sequences d_m and b_m satisfy the following cross-correlation properties

$$r_{db}(m) = \sum_{n=0}^{N_c-1} d_{(n+m) \bmod N_c} \overline{b_n} = \begin{cases} N_c + 1, & \text{if } m = l \cdot N_c \\ & \text{with } l \in \mathbb{Z} \\ 0, & \text{otherwise,} \end{cases}$$

where the overbar denotes complex conjugation. Several choices for the sequences d_m and b_m are discussed in [9].[1]

The (mobile) sounding unit is assumed to be in the far field of the antenna array so that the impinging wavefronts are approximately planar. For simplicity, we assume that a uniform rectangular array (URA) of omnidirectional sensors is located at the receiver. Extensions to other 2-D centro-symmetric array geometries with a dual invariance structure and arbitrary (but identical) sensor characteristics are straightforward [3]. Assume that the URA contains M_1 sensors in x-direction and M_2 sensors in y-direction such that the noise-corrupted array measurements at time t are contained in the matrix $\mathcal{X}_{2D}(t)$, which is of size $M_1 \times M_2$. Due to multipath propagation, d narrowband planar wavefronts of wavelength λ, azimuth ϕ_i, elevation θ_i, and complex amplitude ξ_i, $1 \leq i \leq d$, are impinging on the URA. Hence, the noise-corrupted measurements $\boldsymbol{x}(t) = \text{vec}\{\mathcal{X}_{2D}(t)\}$ may be modeled as

$$\begin{aligned} \boldsymbol{x}(t) &= \sum_{i=1}^{d} \xi_i \cdot \boldsymbol{a}(\mu_i^{(1)}, \mu_i^{(2)}) \cdot s(t - \tau_i) + \boldsymbol{n}(t) \\ &= \boldsymbol{A}_{2D} \cdot \boldsymbol{\Xi} \cdot \boldsymbol{s}(t) + \boldsymbol{n}(t), \end{aligned} \tag{2}$$

where the 2-D array steering matrix

$$\boldsymbol{A}_{2D} = \left[\begin{array}{cccc} \boldsymbol{a}(\mu_1^{(1)}, \mu_1^{(2)}) & \boldsymbol{a}(\mu_2^{(1)}, \mu_2^{(2)}) & \cdots & \boldsymbol{a}(\mu_d^{(1)}, \mu_d^{(2)}) \end{array} \right]$$

contains the 2-D directional information. Here, $\text{vec}\{\boldsymbol{A}\}$ denotes a vector-valued function that maps an $m \times n$ matrix $\boldsymbol{A}$ into an mn-dimensional column vector by stacking the columns of the matrix. The spatial frequencies in x-direction $\mu_i^{(1)} = (2\pi/\lambda)\Delta_x u_i$ and the spatial frequencies in y-direction $\mu_i^{(2)} = (2\pi/\lambda)\Delta_y v_i$ are scaled versions of the corresponding direction cosines $u_i = \cos\phi_i \sin\theta_i$ and $v_i = \sin\phi_i \sin\theta_i$ of the ith source relative to the x- and y-axes, $1 \leq i \leq d$, as illustrated in Figure 1. Moreover, Δ_x and Δ_y are the distances between the sensors in x- and y-direction. Note that the 2-D array steering vectors can be written as Kronecker products of 1-D Vandermonde vectors,

$$\boldsymbol{a}(\mu_i^{(1)}, \mu_i^{(2)}) = \boldsymbol{a}(\mu_i^{(2)}) \otimes \boldsymbol{a}(\mu_i^{(1)}), \quad \text{where}$$

$$\boldsymbol{a}(\mu_i^{(r)}) = \left[\begin{array}{cccc} 1 & e^{\mathrm{j}\mu_i^{(r)}} & \cdots & e^{\mathrm{j}(M_r-1)\mu_i^{(r)}} \end{array} \right]^T, \tag{3}$$

$r = 1, 2$. Furthermore, $\boldsymbol{\Xi} = \text{diag}\{\xi_i\}_{i=1}^d$ is a diagonal matrix containing the amplitudes and phase shifts ξ_i of the d multipath components. Corresponding to the d spatial frequency pairs $\mu_i^{(1)}$ and $\mu_i^{(2)}$, the vector

$$\boldsymbol{s}(t) = \left[\begin{array}{cccc} s(t-\tau_1) & s(t-\tau_2) & \cdots & s(t-\tau_d) \end{array} \right]^T \tag{4}$$

contains d delayed versions of the sounding signal $s(t)$. Here, τ_i denotes the unknown propagation delay of the ith propagation path. Recall that the proposed 3-D channel sounder jointly estimates the 3-D parameters of the dominant wavefronts, i.e., their 2-D spatial frequencies $\mu_i^{(1)}$ and $\mu_i^{(2)}$ as well as their propagation delays τ_i.

2.2. Generation of the Temporal Invariance Structure

Let $r_{pp}(\tau) = \text{E}\{p(t+\tau)p(t)\}$ be the autocorrelation function of the chip waveform $p(t)$ such that the cross-correlation function of the periodic sounding signal $s(t)$ defined in (1) with the correlator sequence

$$c(t) = \sum_{m=1}^{N_c} b_m p(t - mT_c).$$

is a periodic repetition of $r_{pp}(\tau)$ with period $T = N_c T_c = \frac{2\pi}{\omega_0}$ according to

$$r_{sc}(\tau) = \text{E}\left\{s(t+\tau)\overline{c(t)}\right\} = (N_c + 1) \sum_{n=-\infty}^{\infty} r_{pp}(\tau - nT). \tag{5}$$

Its Fourier series will be denoted as

$$R_{sc}(n) = \frac{\omega_0}{2\pi} \int_{-\pi/\omega_0}^{\pi/\omega_0} r_{sc}(\tau) e^{-\mathrm{j}n\omega_0\tau} d\tau.$$

Then it is well known that the Fourier series of $r_{sc}(\tau - \tau_i)$ is given by $e^{-\mathrm{j}n\omega_0\tau_i} R_{sc}(n) = e^{\mathrm{j}n\mu_i^{(3)}} R_{sc}(n)$, where $\mu_i^{(3)} = -2\pi\tau_i/T$ and the propagation delay $\tau_i < T$. If $r_{sc}(\tau)$ and $r_{sc}(\tau - \tau_i)$ are sampled above Nyquist rate, this property still holds for the DFTs of the resulting sequences.

Assume that the array measurements $\boldsymbol{x}(t)$ are sampled at rate $f_s = \frac{M_c}{T_c}$, where the number of samples per chip M_c is an integer. If one samples above Nyquist rate, the correlator (5) can also be realized in the discrete time domain. Using $N_c M_c$ samples of the correlator output, we perform an $(N_c M_c)$-point DFT for each antenna as illustrated in Figure 2. Note that only the spectral lines that correspond to the M_3 largest values of $R_{sc}(n)$ are computed. Thereby, the influence of the additive noise and the computational complexity can be reduced significantly. Let each row of $\mathcal{X}_{\text{cor}}(n) \in \mathbb{C}^{(M_1 M_2) \times (N_c M_c)}$ contain $N_c M_c$ samples of the output of the corresponding antenna after the correlator. The transformation of the space-time channel model to a space-frequency channel model is achieved by post-multiplying $\mathcal{X}_{\text{cor}}(n)$ by the $(N_c M_c) \times M_3$ DFT matrix $\boldsymbol{W}$ such that $\mathcal{X}(n) = \mathcal{X}_{\text{cor}}(n)\boldsymbol{W}$. It is well known that each column of $\boldsymbol{W}$ is of the form

$$\boldsymbol{w}_\ell = \left[\begin{array}{ccccc} 1 & e^{-\mathrm{j}\ell\omega_0} & e^{-\mathrm{j}2\ell\omega_0} & \cdots & e^{-\mathrm{j}(M_c N_c - 1)\ell\omega_0} \end{array} \right]^T.$$

Here, the columns of $\boldsymbol{W}$ compute $M_3 \leq (N_c M_c)$ spectral lines centered at DC according to

$$\boldsymbol{W} = \left[\begin{array}{ccccc} \boldsymbol{w}_{N_c M_c - (M_3-1)/2} & \cdots & \boldsymbol{w}_0 & \cdots & \boldsymbol{w}_{(M_3-1)/2} \end{array} \right],$$

where we have invoked the wrap-around property of the DFT matrix. The construction of the space-frequency data matrix $\mathcal{X}(n)$ is also illustrated in Figure 2. Due to the described Fourier properties and the

[1] The sequences d_m and b_m might, for example, be realized as shifted m-sequences such that $d_m = b_m, \forall m$ [11, 9]. In this case, the correlators of Figure 2 are matched filters which provide the optimum signal to noise ratio (SNR) at their outputs.

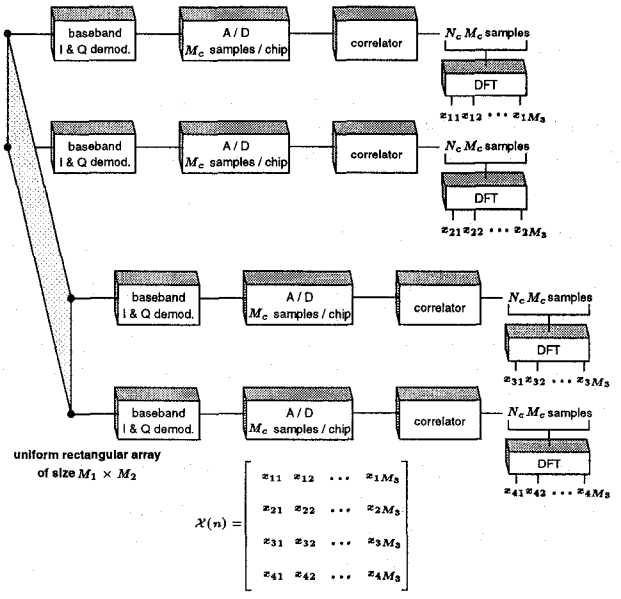

Figure 2: Generation of the 3-D invariance structure using a uniform rectangular array of size $M_1 \times M_2 = 2 \times 2$. Here, $M_3 \leq N_c M_c$ spectral lines are calculated in the frequency domain. Then 3-D Unitary ESPRIT in element space or DFT beamspace is applied to the results obtained from N periods of the spreading sequence $\mathcal{X}(n)$, $1 \leq n \leq N$. Alternatively, a sliding window can be used as well.

data model in (2), $\mathcal{X}(n)$ can be expressed as

$$\mathcal{X}(n) = \sum_{i=1}^{d} \xi_i \cdot \boldsymbol{a}(\mu_i^{(1)}, \mu_i^{(2)})\, \boldsymbol{a}(\mu_i^{(3)})^T \boldsymbol{\Lambda} + \mathcal{N}(n), \qquad (6)$$

where $\mathcal{N}(t)$ contains the additive noise in the space-frequency domain, the Vandermonde vector $\boldsymbol{a}(\mu_i^{(3)})$ is defined in (3), and

$$\boldsymbol{\Lambda} = \operatorname{diag}\left\{R_{sc}(n)\right\}_{n=N_c M_c-(M_3-1)/2}^{(M_3-1)/2}.$$

Apart from this diagonal matrix $\boldsymbol{\Lambda}$, $\mathcal{X}(n)$ may be interpreted as a single snapshot of a (virtual) uniform cube array of the size $M_1 \times M_2 \times M_3$ corresponding to the nth repetition of the spreading sequence in (1). Assuming that the channel is time-invariant during N periods of the spreading sequence $w(t)$, we, therefore, define the matrix

$$\boldsymbol{X} = \left[\ \operatorname{vec}\left\{\mathcal{X}(1)\boldsymbol{\Lambda}^{-1}\right\} \quad \operatorname{vec}\left\{\mathcal{X}(2)\boldsymbol{\Lambda}^{-1}\right\} \quad \cdots \quad \operatorname{vec}\left\{\mathcal{X}(N)\boldsymbol{\Lambda}^{-1}\right\}\ \right],$$

which is of size $M \times N$, where $M = (M_1 M_2 M_3)$. If desired, 3-D space-frequency smoothing (using subarrays of size $M_{\text{sub}_1} \times M_{\text{sub}_2} \times M_{\text{sub}_3}$) can be applied to $\boldsymbol{X}$ as explained in [5].

2.3. 3-D Unitary ESPRIT with Colored Noise

It is the goal of the described 3-D channel sounder to provide high-resolution estimates of the d three-dimensional frequency triplets $\mu_i^{(1)}$, $\mu_i^{(2)}$, and $\mu_i^{(3)}$. A very simple and efficient solution is provided by *3-D Unitary ESPRIT*. If we assume ergodicity, the space-frequency covariance matrix may be estimated as[2] $\boldsymbol{R}_{xx} = \frac{1}{N} \cdot \boldsymbol{X}\boldsymbol{X}^H$. Moreover, the corresponding noise covariance matrix

$$\boldsymbol{R}_{nn} = \mathrm{E}\left\{\operatorname{vec}\left\{\mathcal{N}(n)\boldsymbol{\Lambda}^{-1}\right\} \operatorname{vec}\left\{\mathcal{N}(n)\boldsymbol{\Lambda}^{-1}\right\}^H\right\} \qquad (7)$$

can be obtained in a similar fashion. In the sequel, 3-D Unitary ESPRIT as presented in [3, 5] is modified slightly to take into account a noise correlation matrix $\boldsymbol{R}_{nn}$ that is not necessarily equal to the scaled identity matrix, i.e., colored noise. To this end, let us define left $\boldsymbol{\Pi}$-real matrices [8, 4] as matrices $\boldsymbol{Q} \in \mathbb{C}^{M \times M}$ satisfying $\boldsymbol{\Pi}_M \overline{\boldsymbol{Q}} = \boldsymbol{Q}$. For any positive integer M, $\boldsymbol{I}_M$ denotes the identity matrix of size $M \times M$ and $\boldsymbol{\Pi}_M$ the $M \times M$ exchange matrix with ones on its antidiagonal and zeros elsewhere. The sparse unitary matrix

$$\boldsymbol{Q}_{2q+1} = \frac{1}{\sqrt{2}} \begin{bmatrix} \boldsymbol{I}_q & \boldsymbol{0} & \mathrm{j}\boldsymbol{I}_q \\ \boldsymbol{0}^T & \sqrt{2} & \boldsymbol{0}^T \\ \boldsymbol{\Pi}_q & \boldsymbol{0} & -\mathrm{j}\boldsymbol{\Pi}_q \end{bmatrix}, \qquad (8)$$

for example, is left $\boldsymbol{\Pi}$-real of odd order. A unitary left $\boldsymbol{\Pi}$-real matrix of size $2q \times 2q$ is obtained from (8) by dropping its center row and center column. More left $\boldsymbol{\Pi}$-real matrices can be constructed by post-multiplying a left $\boldsymbol{\Pi}$-real matrix $\boldsymbol{Q}$ by an arbitrary real matrix $\boldsymbol{R}$, i.e., every matrix $\boldsymbol{Q}\boldsymbol{R}$ is left $\boldsymbol{\Pi}$-real.

In the first step of Unitary ESPRIT, forward-backward averaging is achieved by transforming the covariance matrices $\boldsymbol{R}_{xx}$ and $\boldsymbol{R}_{nn}$ to real matrices according to

$$\boldsymbol{G}_{xx} = \operatorname{Re}\left\{\boldsymbol{Q}_M^H \boldsymbol{R}_{xx} \boldsymbol{Q}_M\right\} \quad \text{and} \quad \boldsymbol{G}_{nn} = \operatorname{Re}\left\{\boldsymbol{Q}_M^H \boldsymbol{R}_{nn} \boldsymbol{Q}_M\right\},$$

where $\boldsymbol{Q}_M$ denotes an arbitrary left $\boldsymbol{\Pi}$-real matrix that is also unitary. Then a basis of the estimated signal subspace $\boldsymbol{E}_s$ is determined through a real-valued generalized eigendecomposition

$$\boldsymbol{G}_{xx}\boldsymbol{E}_s = \boldsymbol{G}_{nn}\boldsymbol{E}_s \cdot \boldsymbol{\Sigma} \quad \text{with} \quad \boldsymbol{\Sigma} = \operatorname{diag}\left\{\sigma_i\right\}_{i=1}^{M}, \qquad (9)$$

where the d dominant generalized eigenvectors of the matrix pair $\boldsymbol{G}_{xx}$ and $\boldsymbol{G}_{nn}$ form the columns of $\boldsymbol{E}_s$. Using the real-valued signal subspace estimate $\boldsymbol{E}_s$, three real-valued invariance equations are formed,

$$\boldsymbol{K}_{(r)1}\boldsymbol{G}_{nn}\boldsymbol{E}_s\boldsymbol{\Upsilon}_r \approx \boldsymbol{K}_{(r)2}\boldsymbol{G}_{nn}\boldsymbol{E}_s \in \mathbb{R}^{m_r \times d}, \qquad (10)$$

$r = 1, 2, 3$, where the three corresponding pairs of selection matrices $\boldsymbol{K}_{(r)1}$ and $\boldsymbol{K}_{(r)1}$ are constructed as described in [3, 5]. The three invariance equations (10) may be solved independently via least squares (LS), total least squares (TLS), or structured least squares (SLS) or jointly via a three-dimensional extension of SLS (3-D SLS), yielding three real-valued matrices $\boldsymbol{\Upsilon}_r \in \mathbb{R}^{d \times d}$, $r = 1, 2, 3$. Note that these matrices are not necessarily symmetric.

In the noiseless case or with an infinite number of sequences N, the three solutions $\boldsymbol{\Upsilon}_r$ of (10) have real-valued eigenvalues and share the same set of real-valued eigenvectors. More specifically, they admit the following eigendecompositions

$$\boldsymbol{\Upsilon}_r = \boldsymbol{T}\,\boldsymbol{\Omega}_r \boldsymbol{T}^{-1} \quad \text{with} \quad \boldsymbol{\Omega}_r = \operatorname{diag}\left\{\tan\left(\frac{\mu_i^{(r)}}{2}\right)\right\}_{i=1}^{d}, \qquad (11)$$

$r = 1, 2, 3$. Notice first that all the matrices in (11) are real-valued. Secondly, the eigenvalues of $\boldsymbol{\Upsilon}_r$, i.e., the diagonal elements of $\boldsymbol{\Omega}_r$, contain the desired frequency information. Thirdly, if the matrix of eigenvectors $\boldsymbol{T} \in \mathbb{R}^{d \times d}$ in the spectral decomposition of $\boldsymbol{\Upsilon}_r$ is the same for all r, the diagonal elements of the matrices $\boldsymbol{\Omega}_r$ and, therefore, also the desired frequencies are automatically paired.

In practice, though, only a finite number N of noise-corrupted sounding sequences is available. Therefore, the three matrices $\boldsymbol{\Upsilon}_r$ do not exactly share the same set of eigenvectors. To determine an approximation of the set of common eigenvectors only from one of the $\boldsymbol{\Upsilon}_r$ is, obviously, not the best solution, since this strategy would rely on an arbitrary choice and would also discard information contained in the other two matrices. Thus, from a statistical point of view, it is desirable, for the sake of accuracy and robustness, to compute the "average eigenstructure" of these matrices. To this end, we use a Jacobi-type method to calculate a simultaneous Schur decomposition of several matrices. The Jacobi type method calculates the orthogonal matrix $\boldsymbol{\Theta}$ such that the R matrices

$$\boldsymbol{U}_r = \boldsymbol{\Theta}^T \boldsymbol{\Upsilon}_r \boldsymbol{\Theta}, \quad 1 \leq r \leq R,$$

[2] Instead of this rectangular window, we may also use a sliding window to compute $\boldsymbol{R}_{xx}$.

are approximately upper triangular in a least squares sense. The diagonal elements of $\boldsymbol{U}_r$ are denoted as $u_{ii}^{(r)}, 1 \le i \le d$. Then automatically paired frequency estimates are obtained as

$$\mu_i^{(r)} = 2 \arctan\left(u_{ii}^{(r)}\right), \quad 1 \le i \le d, \quad 1 \le r \le R.$$

Further details are found in [3, 5].

2.4. Estimation of the Amplitudes

If the array geometry is known and the array is calibrated, the 2-D steering matrix $\boldsymbol{A}_{2D}$ is completely specified by the estimated spatial frequencies $\mu_k^{(1)}$ and $\mu_k^{(2)}$. Fast fading influences the amplitudes over short intervals, whereas DOAs and delays remain constant over longer periods. We, therefore, estimate the amplitudes over Q sequences, where Q might be significantly smaller than N. To this end, let us collect QN_cM_c samples of $\boldsymbol{x}(t)$ as defined in (2). Then the resulting matrix $\boldsymbol{X}_Q \in \mathbb{C}^{(M_1M_2)\times(QN_cM_c)}$ may be expressed as

$$\boldsymbol{X}_Q = \boldsymbol{A}_{2D} \cdot \boldsymbol{\Xi} \cdot \boldsymbol{S} + \boldsymbol{N}_Q. \tag{12}$$

Hence, the linear minimum variance unbiased estimate of the amplitudes $\boldsymbol{\xi} = \begin{bmatrix} \xi_1 & \xi_2 & \dots & \xi_d \end{bmatrix}^T$ is given by

$$\boldsymbol{\xi} = \left(\boldsymbol{B}^H \boldsymbol{R}_{NN}^{-1} \boldsymbol{B}\right)^{-1} \boldsymbol{B}^H \boldsymbol{R}_{NN}^{-1} \cdot \mathrm{vec}\{\boldsymbol{X}_Q\},$$

where $\boldsymbol{R}_{NN} = \mathrm{E}\{\mathrm{vec}\{\boldsymbol{N}_Q\}\mathrm{vec}\{\boldsymbol{N}_Q\}^H\}$, $\boldsymbol{B} = \boldsymbol{S}^T \diamond \boldsymbol{A}_{2D}$, and the Khatri-Rao product $\diamond$ denotes the columnwise Kronecker product.

3. Simulations

In the simulations, we have used a chip waveform with a square-root raised cosine spectrum and a rolloff factor of $\beta = 0.22$.

First, a URA of size $M_1 \times M_2 = 2 \times 2$ with $\Delta_x = \Delta_y = 0.45\lambda$ was employed. Two wavefronts ($\phi_1 = 10°, \theta_1 = 0°, \tau_1 = 5 \cdot T_c$, and $\phi_2 = 30°, \theta_2 = 0°, \tau_2 = 5.5 \cdot T_c$) with equal power were impinging on the array. The RMS error of the estimated spatial frequencies (averaged over both wavefronts) was used to compare the performance of the proposed channel sounder based on 3-D Unitary ESPRIT with a channel sounder based on 2-D Unitary ESPRIT as described in [2]. Figure 3 depicts the results as a function of the SNR

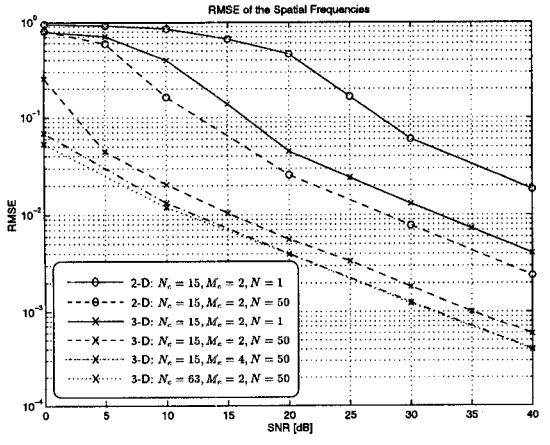

Figure 3: RMS error (RMSE) of the spatial frequencies averaged over both wavefronts ($\phi_1 = 10°, \theta_1 = 0°, \tau_1 = 5 \cdot T_c$, and $\phi_2 = 30°, \theta_2 = 0°, \tau_2 = 5.5 \cdot T_c$) as a function of the SNR (averaged over 500 trials). The circles (o) denote joint 2-D estimation of the spatial frequencies via 2-D Unitary ESPRIT, whereas the crosses (x) denote joint 3-D estimation of the spatial and temporal frequencies via 3-D Unitary ESPRIT ($M_1 \times M_2 = 2 \times 2$, $M_3(N_c = 15) = 11$, $M_3(N_c = 63) = 51$, $\Delta_x = \Delta_y = 0.45\lambda$, $M_{\mathrm{sub}_1} = M_{\mathrm{sub}_2} = 2$, $M_{\mathrm{sub}_3} = 5$).

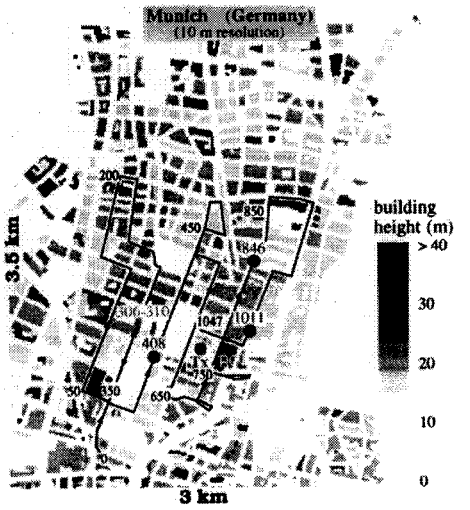

Figure 4: Rastered map of downtown Munich showing the location of the base station (Tx) and a route containing 1050 measurement points ($\approx$ 13.5 km).

averaged over 500 trials for different values of the spreading sequence length N_c, the oversampling factor M_c, and the number of spreading sequences N used for the joint parameter estimation. Here, the circles (o) denote joint 2-D estimation of the spatial frequencies via 2-D Unitary ESPRIT, whereas the crosses (x) denote joint 3-D estimation of the spatial and temporal frequencies via 3-D Unitary ESPRIT.

Finally, we present simulation results that use realistic 2-D arrival angles derived from a ray tracing program for macrocell environments [7]. They are based on a three-dimensional topographical model of downtown Munich, where the height of the base station was 26 meters and the height of the transmitter at the mobiles 2 meters. The heights of most buildings varied between 10 and 30 meters as depicted in Figure 4. In this urban environment, the propagation conditions at 1 GHz were predicted via 3-D ray tracing, taking into account wave interactions like diffraction and scattering over each propagation path [7]. Ray tracing tools developed at the University of Karlsruhe provided the channel impulse response of each propagation path in terms of its attenuation, time delay, 2-D launching angle (at the transmitter), and 2-D arrival angle (at the receiver). The resulting coverage predictions agree with measurements taken in the same urban area.

In the simulations, a random phase shift was assigned to each propagation path. Here, a URA of $M_1 \times M_2 = 5 \times 5$ antennas with $\Delta_x = \Delta_y = 0.45\lambda$ was used at the base station (which is denoted by the symbol Tx in Figure 4). As an illustrative example, consider sounding position 846. The top row of Figure 5 depicts the corresponding power of the impinging wavefronts as a function of the 2-D arrival angles (direction cosines) and the corresponding propagation delays in the u-v plane (on the left side) and in the azimuth-delay (ϕ-τ) plane (on the right side) as predicted via the ray tracing tool. The bottom row of the same figure shows the estimation results obtained with the proposed channel sounder based on 3-D Unitary ESPRIT. Clearly, the dominant 2-D arrival angles, the corresponding propagation delays, and the corresponding amplitudes are estimated correctly.

4. Efficient Space-Frequency Processing in DS-CDMA Systems

Using slight modifications, the described 3-D high-resolution procedure may also be used on the *uplink* of a direct sequence CDMA system to determine the 3-D parameters of the mobile radio channel between the desired user and the base station in an efficient fashion. To this end, estimates of the space-frequency correlation matrix of the desired and the interfering user ($\boldsymbol{R}_{xx}$) and the space-frequency correlation matrix of the interfering users alone ($\boldsymbol{R}_{nn}$) should be obtained

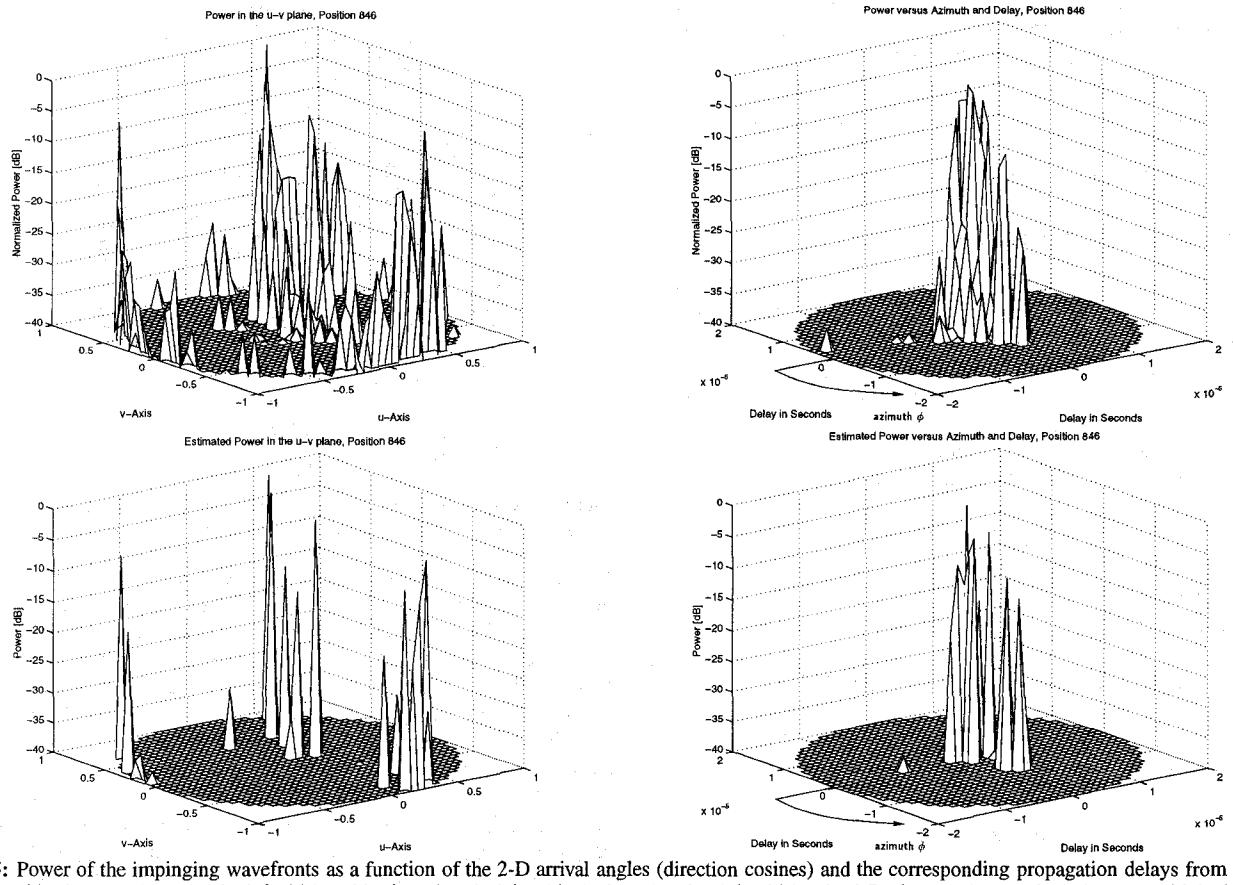

Figure 5: Power of the impinging wavefronts as a function of the 2-D arrival angles (direction cosines) and the corresponding propagation delays from sounding position 846 in the u-v plane (on the left side) and in the azimuth-delay (ϕ-τ) plane (on the right side). The 3-D plots on the top show the power of the impinging wavefronts as predicted via ray tracing, whereas the bottom row visualizes the 3-D estimates obtained by applying the proposed 3-D channel sounder (simulation parameters: $M_1 \times M_2 = 5 \times 5$, $\Delta_x = \Delta_y = 0.45\lambda$, $M_c = 10$, $N_c = 31$, $M_3 = 24$, $M_{\text{sub}_1} = M_{\text{sub}_2} = 5$, $M_{\text{sub}_3} = 10$, $T_c = 0.71$ μs, $f_c = 1$ GHz, $N = 500$, $Q = 10$, SNR $= 20$ dB). Clearly, the dominant 2-D arrival angles, the corresponding propagation delays, and the corresponding amplitudes are estimated correctly.

as specified in [12]. Then 3-D Unitary ESPRIT can be used to to estimate the 2-D arrival angles and the corresponding propagation delays of the dominant wavefronts of the desired user as explained in Subsection 2.3. In an FDD system, the estimated 2-D arrival angles of the desired user should, subsequently, be used for efficient *downlink* beamforming.

Concluding Remarks

We have presented an efficient high-resolution channel sounder that jointly estimates the 2-D arrival angles and the corresponding propagation delays via a closed-form procedure based on the element space version of 3-D Unitary ESPRIT. The simulation results for the synthetic and especially for the realistic scenarios (that are based on parameters generated by a ray tracing tool) illustrate the excellent performance of the presented 3-D channel sounding scheme.

If one desires to operate in a lower dimensional beamspace to focus on a particular (space-frequency) sector of interest, the proposed 3-D channel sounder can also operate with the *DFT beamspace version* of 3-D Unitary ESPRIT [3] instead of the *element space version* described in this paper.

References

[1] B. Fleury, D. Dahlhaus, R. Heddergott, and M. Tschudin, "Wideband angle of arrival estimation using the SAGE algorithm", in *Proc. IEEE ISSSTA*, vol. 1, pp. 79–85, Mainz, Germany, Sept. 1996.

[2] J. Fuhl, J. P. Rossi, and E. Bonek, "High-resolution 3D direction-of-arrival determination for urban mobile radio", *IEEE Trans. Antennas and Propagation*, vol. 45, pp. 672–682, Apr. 1997.

[3] M. Haardt, *Efficient One-, Two-, and Multidimensional High-Resolution Array Signal Processing*, Shaker Verlag, Aachen, Germany, 1996, ISBN 3-8265-2220-6.

[4] M. Haardt and J. A. Nossek, "Unitary ESPRIT: How to obtain increased estimation accuracy with a reduced computational burden", *IEEE Trans. Signal Processing*, vol. 43, pp. 1232–1242, May 1995.

[5] M. Haardt and J. A. Nossek, "Simultaneous Schur decomposition of several nonsymmetric matrices to achieve automatic pairing in multidimensional harmonic retrieval problems", *IEEE Trans. Signal Processing*, vol. 46, Jan. 1998, scheduled to appear.

[6] A. Klein, W. Mohr, R. Thomas, P. Weber, and B. Wirth, "Direction-of-arrival of partial waves in wideband mobile radio channels for intelligent antenna concepts", in *Proc. IEEE Vehicular Techn. Conf.*, vol. 2, pp. 849–853, Atlanta, GA, Apr. 1996.

[7] T. Kürner, D. C. Cichon, and W. Wiesbeck, "Concepts and results for 3D digital terrain-based wave propagation models: An overview", *IEEE Journal on Selected Areas in Communications*, vol. 11, pp. 1002–1012, Sept. 1993.

[8] A. Lee, "Centrohermitian and skew-centrohermitian matrices", *Linear Algebra and its Applications*, vol. 29, pp. 205–210, 1980.

[9] U. Martin, *Ausbreitung in Mobilfunkkanälen: Beiträge zum Entwurf von Meßgeräten und zur Echoschätzung*, Ph. D. dissertation, University of Erlangen, Erlangen, Germany, Oct. 1994, in German.

[10] U. Martin, "A directional radio channel model for densely build-up urban area", in *Proc. 2nd European Personal Mobile Communications Conference*, pp. 237–244, Bonn, Germany, Sept. 1997.

[11] U. Martin, H. W. Schüßler, and K. Schwarz, "Ein System zur Messung der Eigenschaften von Mobilfunkkanälen und ein Verfahren zur Nachverarbeitung der Meßdaten", *Frequenz*, vol. 46, pp. 178–188, 1992.

[12] M. D. Zoltowski, J. Ramos, C. Chatterjee, and V. Roychowdhury, "Blind adaptive 2D rake receiver for DS-CDMA based on space-frequency MVDR processing", *IEEE Trans. Signal Processing*, June 1996, submitted for publication.